Chapter 12

Device Integrity of Drug-eluting Depot Stent for Smart Drug Delivery

Hao-Ming Hsiao, Aichi Chien, Bor-Hann Huang, Dian-Ru Li, Hsin Chen and Chun-Yi Ko

Additional information is available at the end of the chapter

http://dx.doi.org/10.5772/61790

Abstract

Atherosclerosis, or hardening of the arteries, is a condition in which plaque, made of cholesterol, fatty substances, cellular waste products, calcium, and fibrin, builds up inside the arteries. A metallic stent is a small mesh tube that is used to treat these narrowed arteries such as coronary artery diseases. The drug-eluting stent has a metallic stent platform coated with drug-polymer mix and has been shown to be superior to its metallic stent counterpart in reducing restenosis. In the past few years, a novel variation of the drug-eluting stent with micro-sized drug reservoirs (depot stent) has been introduced to the market. It allows smart programmable drug delivery with spatial/temporal control and has potential advantages over conventional stents. The drug-polymer mix compound can be altered from one reservoir to the next, allowing a highly-controlled release of different medications. For example, this depot stent concept can be applied in the renal indication for potential treatment of both renal artery stenosis (upstream) and its associated kidney diseases (downstream) simultaneously. However, the creation of such drug reservoirs on the stent struts inevitably compromises its mechanical integrity. In this study, the effects of these drug reservoirs on stent key clinical attributes were systematically investigated. We developed finite element models to predict the mechanical integrity of a balloon-expandable stent at various stages of its function life such as manufacturing and acute deployment, as well as the stent radial strength and chronic fatigue life. Simulation results show that (1) creating drug reservoirs on a stent strut could impact the stent fatigue resistance to certain degrees; (2) drug reservoirs on the high stress concentration regions led to much greater loss in all key clinical attributes than reservoirs on other locations; (3) reservoir shape change resulted in little differences in all key clinical attributes; and (4) for the same drug loading capacity, larger and fewer reservoirs yielded

higher fatigue safety factor. These results can help future stent designers to achieve the optimal balance of stent mechanical integrity and smart drug delivery, thereby opening up a wide variety of new opportunities for disease treatments. We also proposed an optimized depot stent with tripled drug capacity and acceptable marginal trade-off in key clinical attributes when compared to the current drug-eluting stents. This depot stent prototype was manufactured for the demonstration of our design concept.

Keywords: Drug-eluting stent, Drug reservoir, Depot stent, Mechanical integrity, Smart drug delivery

1. Introduction

Percutaneous coronary intervention (PCI), also known as angioplasty, has been the current standard for the treatment of coronary artery diseases. A metallic stent is a tiny, coiled wire-mesh tube that can be deployed into an artery and expanded using a catheter during angioplasty to open a narrowed artery. However, intimal cells can proliferate due to the artery injury during stenting, often leading to in-stent restenosis of the artery. Restenosis, the re-narrowing of the artery after the intervention, is the most common occurrence after angioplasty procedures in early days [1-3].

In the past decade, stent technology has evolved from the metallic stent to the so-called drug-eluting stent (DES). A drug-eluting stent has a metallic stent platform coated with an anti-proliferative drug (e.g., Sirolimus or Everolimus) that is known to interfere with the restenosis process. The drug is typically mixed with a polymer compound (durable or biodegradable) to precisely control its release rate and timing to the artery wall. The adoption of the drug-eluting stent has resulted in a dramatic lowering in restenosis rates from 20 to 30% for the metallic stent to the single digit now [4, 5], leading to a worldwide embrace of this new technology in healthcare. Since the introduction of the drug-eluting stent, restenosis has become less of an issue for the treatment of coronary artery diseases. The drug-eluting stent has thus become the gold standard for PCI procedures since then.

Although the drug-eluting stent has been hugely successful in lowering restenosis, the stenting technology continues to evolve in a quest for better solutions. The biodegradable vascular scaffold (BVS) presents the next frontier. Biodegradable stents stay in the blood vessel for a limited period of time, give mechanical support, and then degrade to non-toxic substances. Potential advantages of having the stent disappear from the treated site include reduced late stent thrombosis, facilitation of repeat treatments to the same site, and freedom from fracture-induced restenosis. The biodegradable stents with poly lactic acid (PLA) have good physical properties such as high strength and processability; and in a suitable disposal site it will degrade to natural products [6-8]. BVS has the potential to act as local drug delivery systems. Therefore, it is possible to design a BVS, not only offering a physical support to the vessel wall, but also presenting a pharmacological approach in the prevention of thrombus formation and intimal proliferation [9-11].

http://dx.doi.org/10.5772/61790

In recent years, another novel concept in smart drug delivery is the emergence of the depot stent: a metallic stent laser-drilled with micro-sized holes, or called "reservoirs," that can be loaded with single or multiple drugs, potentially in various doses or formulations [12, 13]. The drug-polymer mix can be varied from one reservoir to the next, allowing a high flexibility of controlled release of different drugs. For example, on the outer side of the reservoirs close to the artery wall, drugs preventing neointimal proliferation can be filled, while on the inner side of the reservoirs close to the blood stream, thrombocyte inhibitors can be filled to prevent stent thrombosis (Figure 1). In addition, it is believed that this stent concept could become even more powerful in some cases such as the renal indication for potential treatment of both renal artery stenosis (RAS) and its associated kidney diseases at the same time, as renal artery stenosis is usually related to progressive hypertension, renal insufficiency, or kidney failure reciprocally. For example, drugs preventing neointimal proliferation can be applied on the outside portion of the reservoirs closer to the artery wall, whereas on the inside portion of the reservoirs, drugs for kidney diseases can be loaded and carried by the blood stream to the distal kidney organ for direct target therapy. This proposed method could potentially help to treat two problems in one attempt. Figure 2 shows that different types of drugs can be administered independently at each stage after intervention.

The depot stent has other advantages. Unlike drug-eluting stents, the depot stent does not need to be surface-coated. Therefore, it is free of surface coating layers, thereby reducing direct contact between the artery wall and the polymer compound. Such contact is believed to increase the potential risk of chronic inflammation or late stent thrombosis. Another advantage is the decrease of the overall stent profile due to the absence of surface coating layers. Lower stent profile allows a stent to access narrower lesion sites and offers physicians easier deliverability. Given these potential advantages, however, creating reservoirs on the stent struts inevitably weaken the stent structure and compromise its mechanical integrity, namely, its abilities to sustain various loading conditions including crimping onto a balloon catheter during manufacturing, stent expansion during deployment, radial resistance to blood vessels from collapsing inward, and long-term fatigue resistance to systolic/diastolic pressure loadings. Therefore, the objective of this paper is to investigate the impact of the micro-sized reservoirs on the overall mechanical integrity of the depot stent.

Computational modeling has emerged as a powerful tool for optimization of stent designs and can be used along with bench testing to improve stent clinical performance [14-18]. Such computational tools could provide valuable insights to various aspects of stent design tactics which may consequently reduce the potential risk of vascular injury and restenosis. It also gives extensive information under a highly-controlled environment, making it feasible to screen numerous design iterations prior to costly prototyping. Therefore, in this study, computational models were developed to assess key clinical attributes of the depot stent using finite element analysis (FEA). Based on these findings, we propose an optimal depot stent design in an effort to increase the drug capacity without significantly comprising its mechanical integrity.

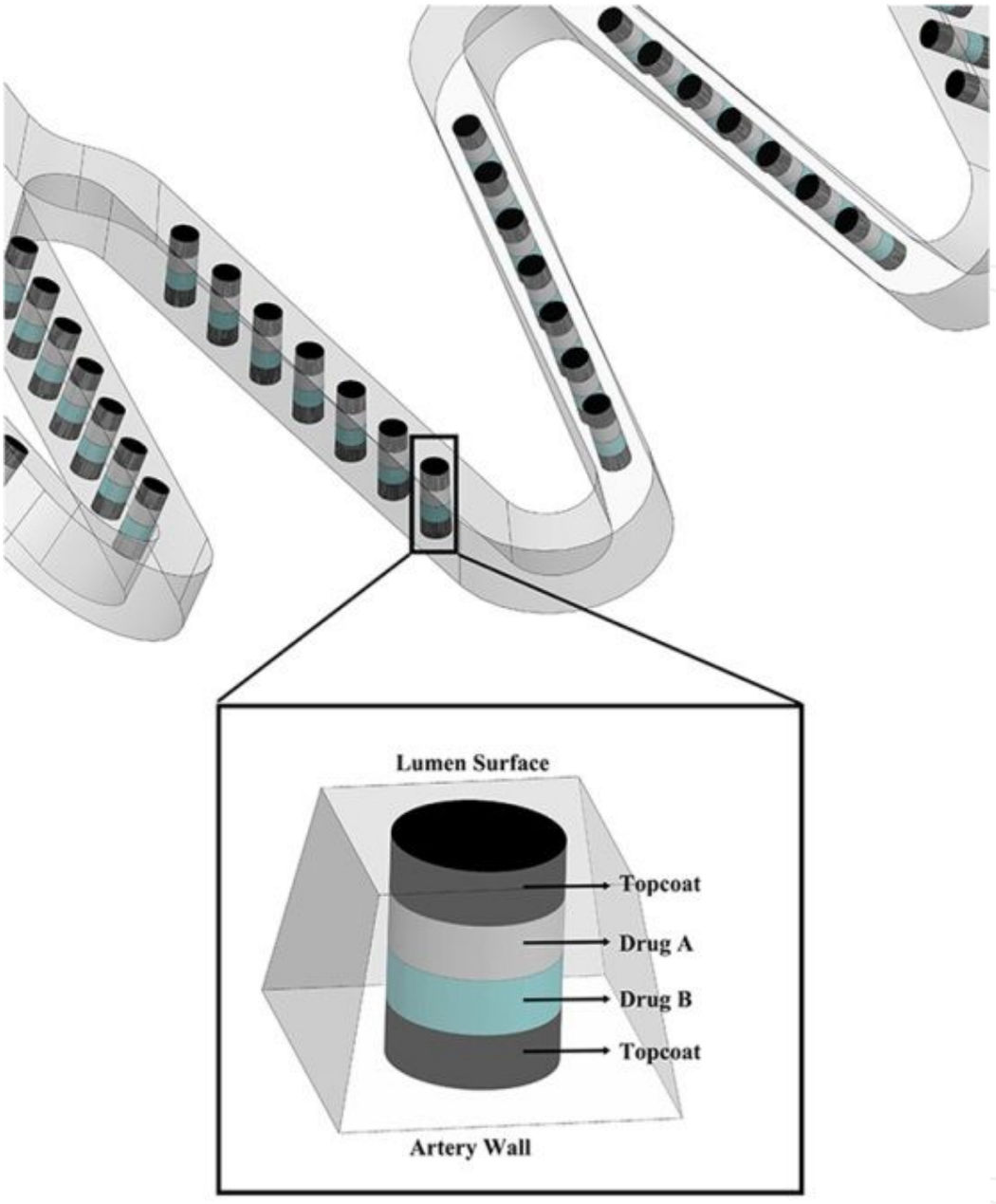

Figure 1. Depot stent concept with different types of drugs and release rates administered independently of opposite sides of the stent.

2. Depot stent configuration

An L-605 cobalt–chromium balloon-expandable stent was used as the "standard" stent for baseline in this study. Micro-sized drug reservoirs were created on this standard stent struts in order to investigate their effects on the stent mechanical integrity. The stent was designed to form a series of nested rings interconnected with bridging connectors (CO). The design parameters such as crown radius (CR) and strut dimension were tailored to optimize the overall stent performance.

http://dx.doi.org/10.5772/61790

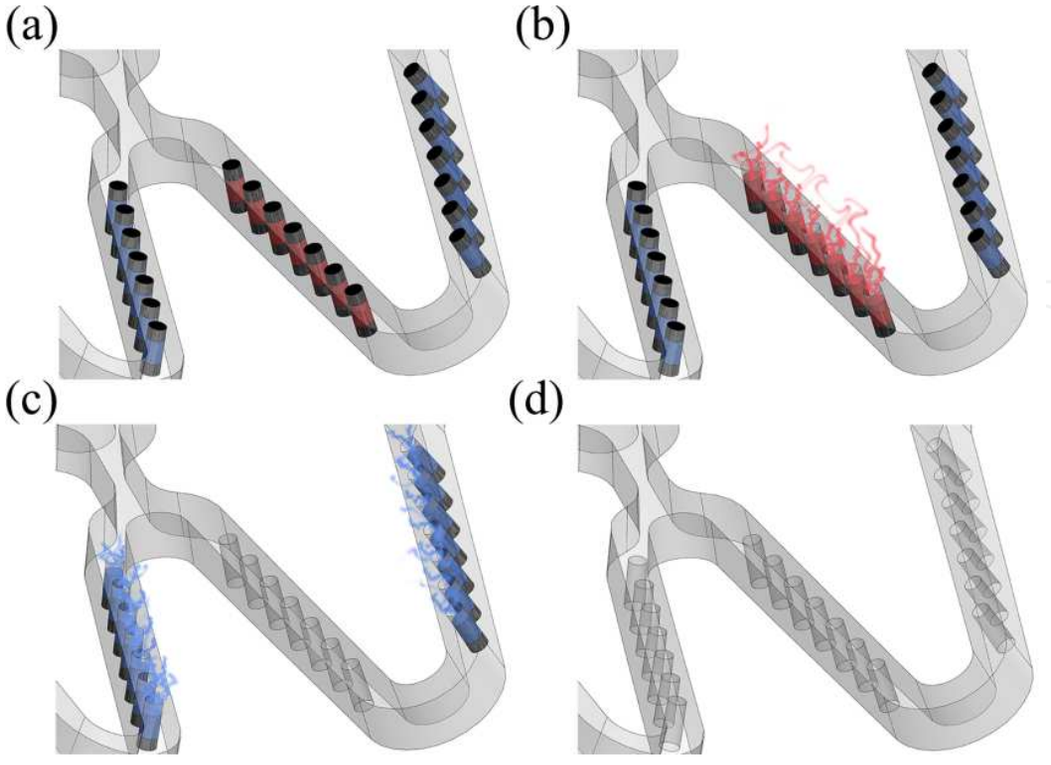

Figure 2. Schematic of sequential release of multiple drugs for each period after intervention.

The standard stent, which has exactly the same geometry as the investigated depot stents but without drug reservoirs, was first evaluated to establish the baseline information. The FEA simulation was then conducted to investigate the effects of reservoir location on the mechanical integrity of the depot stent. Five equally spaced circular (cylindrical if considering depth) reservoirs were created on three major locations of the depot stent, namely, connectors, bar arms (BA), and crowns (Figure 3). The diameter of each circular reservoir was 50% of the strut width, whereas the reservoir depth was varied for evaluation. The spacing between two adjacent reservoirs was 0.15 mm, as defined by the length between two reservoir centers along the strut centerline. The choice of the reservoir number and size was based on the condition that the total reservoir capacity of the drug–polymer mix inside the reservoirs of the depot stent was able to fully replace the total volume of surface coating layers on a typical drug-eluting stent with an average coating thickness of 5μm [4].

Since adding more reservoirs increases the total drug capacity, investigation was also carried out on the depot stent with reservoirs uniformly spread on the entire stent to understand whether the mechanical integrity of such a depot stent is further compromised or not (Figure 3(d)). In this special case, the entire stent was covered by reservoirs with the same circular diameter and depth aforementioned. Another method of increasing the total drug capacity is by drilling through-holes instead of blind-holes into the stent struts. Therefore, FEA simulation was also conducted to investigate the effects of reservoir depth on the mechanical integrity. Further studies were conducted on the depot stent to investigate whether the reservoir shape, size, and number affect the stent mechanical integrity or not.

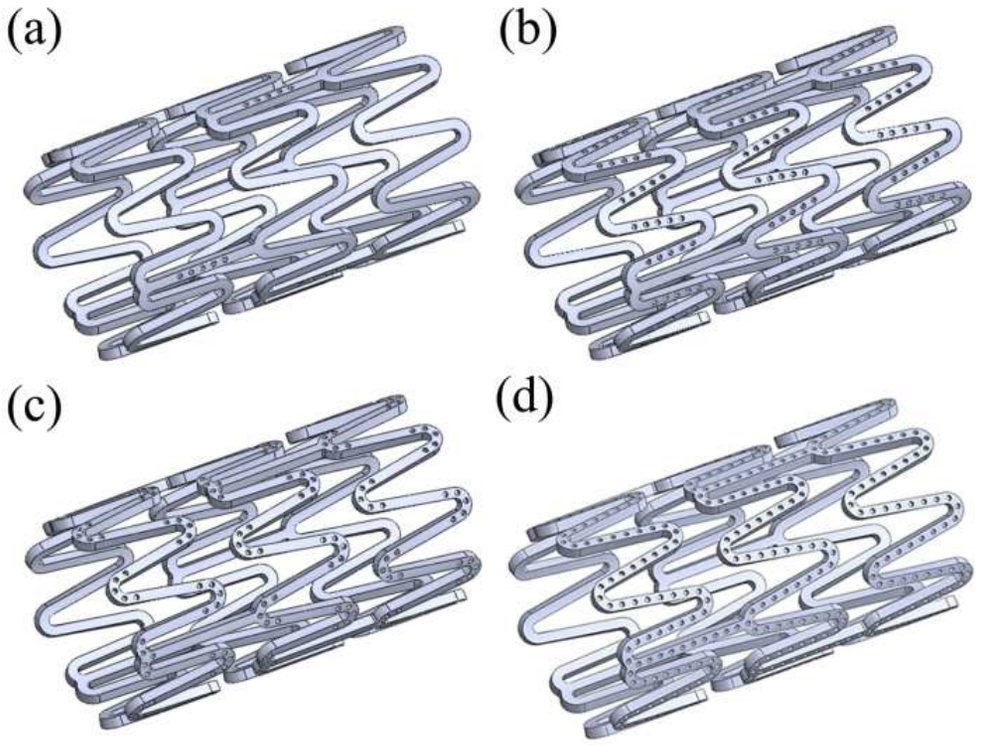

Figure 3. Depot stent with reservoirs on (a) connectors, (b) bar arms, (c) crowns, and (d) entire stent surfaces.

3. Computational model development

3.1. Stent mechanical integrity assessment

On 18 April 2010, the US Food and Drug Administration (FDA) published an official document, "Non-Clinical Engineering Tests and Recommended Labeling for Intravascular Stents and Associated Delivery Systems," to serve as a guide for the medical device industry. In addition to the routine stent dimensional tests such as dimensional verification, percent surface area, foreshortening, and recoil, this document lists several key clinical relevant functional attributes in which the FDA is interested when reviewing future new stent submissions. For the balloon-expandable stent, these key clinical attributes include radial strength, stresses–strains, and fatigue resistance. Each of these properties can serve as an indicator with respect to various aspects of the stent integrity. In this study, three key clinical attributes were used to assess the mechanical integrity of the depot stent.

3.1.1. Radial Strength (RS)

One of the most important functions of the stent is to create a scaffolding structure in the artery and exert radial force against the artery wall to prevent its reclosure. Radial strength represents the ability of a stent to resist radial collapse under external pressure loadings exerted by the artery wall. It is defined as the maximum pressure at which the stent experiences irreversible deformation.

http://dx.doi.org/10.5772/61790

3.1.2. Equivalent plastic strain (PEEQ)

Since the in vivo deployment of a balloon-expandable stent involves large plastic deformation, the equivalent plastic stresses and strains have to be calculated throughout the stent. This stress analysis provides a risk assessment of acute device failure. The stress or strain contour plots provide the overall distribution of plastic stresses or strains and identify the most fracture-prone locations of a stent. Stent fracture may cause loss of the radial strength or perforation of the blood vessel by the fractured stent struts.

3.1.3. Fatigue Safety Factor (FSF)

Stent fracture due to long-term pulsatile fatigue loading may result in loss of the radial strength, thrombus formation, focal restenosis, or perforation of the blood vessel by the fractured stent struts. FDA recommends using a Goodman life analysis to determine the fatigue resistance of a stent to clinically relevant pressure loadings up to 4×108 cycles. The Goodman life analysis, combined with the stress analysis aforementioned and accelerated fatigue bench testing, provides a comprehensive risk assessment of long-term stent durability. The resulting fatigue safety factor shows how safe a stent is from fatigue failure based on the Goodman life analysis.

3.2. Finite element analysis

3.2.1. Finite element model

A stent deployed in the vasculature system is subjected to various loading modes which may consequently compromise the stent mechanical integrity during its service life. In this study, finite element models were developed to evaluate the mechanical integrity and fatigue resistance of a stent to various loading conditions involved in manufacturing and deploying a stent consistent with the current practice. The entire stress–strain history of the stent in each loading step was considered to incorporate the effects of accumulated residual stress–strains throughout the procedures. It includes manufacturing (crimped onto a balloon catheter), in vivo deployment (expanded into an artery), and their corresponding recoil and pulsatile loading subjected to systolic/diastolic pressures. The FEA simulation determines the distribution of stress and strain, fatigue safety factor, and radial strength imposed by the following steps:

Step 1. Crimping a stent from 2.54 mm to 2 mm OD (crimp).

Step 2. Removing outer constraint to allow stent recoil after crimping (crimp-recoil).

Step 3. Expanding a stent to 6.0 mm ID (expansion).

Step 4. Removing inner constraint to allow stent recoil after expansion (expansion-recoil).

Step 5. Applying 180/80 mmHg systolic/diastolic pressures for stent fatigue assessment (or applying external pressure for radial strength assessment).

It should be noted that step 5 can be used to calculate either the fatigue safety factor or radial strength of a stent.

3.2.2. Stent geometry and meshing

The ABAQUS/standard finite element solver (Dassault Systemes Simulia Corp., Providence, RI, USA) was used to perform the stent FEA analysis. Since a stent has repeated patterns in its axial and circumferential directions, three representative rings instead of the entire stent were modeled to save computational time (Figure 3). In order to simulate the manufacturing (crimp onto a balloon catheter) and in-vivo deployment (expansion inside an artery) steps, two rigid cylinders with diameters of 2.54 and 1.12 mm were incorporated into the stent model with one cylinder inside the stent and the other one outside the stent. Gervaso et al. and De Beule et al. demonstrated that using the displacement-control expansion of a rigid cylinder for simulation of a balloon expansion could provide reliable and accurate information regarding the stent shape, stress–strain behavior, etc., when reaching the stent nominal diameter [19, 20]. Therefore, the displacement-control simplification was used in this study, as it is computationally less expensive than simulations involving balloon-driven expansion. Our goal is to assess the impact of drug reservoirs to the "standard" stent on a relative scale, so the displacement-control expansion serves that purpose well.

The stent model was meshed with the eight-node linear brick element in incompatible mode (C3D8I) with the element size of one-sixth of the strut width and one-third of strut thickness. This specific mesh size was chosen after a mesh sensitivity study to ensure that stress–strain variation on the stent was adequately captured. The inside and outside rigid cylinders were meshed with the four-node quadrilateral surface element (SFM3D4).

3.2.3. Material properties and boundary conditions

The material properties of L-605 cobalt–chromium alloy along with the ABAQUS von Mises plasticity model with isotropic hardening for large deformation analysis were used. Its Young's modulus, Poisson ratio, yield stress, ultimate stress, ultimate strain, and fatigue endurance limit are 203 GPa, 0.3, 590 MPa, 1689 MPa, 60%, and 483 MPa, respectively.

A frictionless contact was used to prevent penetration between two surfaces of the model during crimping and expansion, with the following contact pairs implemented:

1. The first contact pair was defined as the surface contact between the inner surface of the outer rigid cylinder and the outer surface of the stent.
2. The second contact pair was defined as the surface contact between the outer surface of the inner rigid cylinder and the inner surface of the stent.
3. The third contact pair was defined as the side contact between any two stent struts during crimping.

3.2.4. Stent stress–strain analysis

In step 1, stress–strain analysis was conducted to simulate the crimping of a stent onto a balloon catheter. The outer rigid cylinder was compressed in the radial direction with the displacement control, forcing the stent to collapse inward. In step 2, stent recoil after crimping due to elastic

http://dx.doi.org/10.5772/61790

strain energy was modeled by removing the outer rigid cylinder to allow for the stent recovery. In step 3, to simulate the in-vivo deployment, the inner rigid cylinder was expanded in the radial direction with the displacement control to simulate the stent deployment to the target size. In the final step, stent recoil after expansion due to elastic strain energy was modeled by removing the inner rigid cylinder to allow for the stent recovery. Figure 4 demonstrates the configuration of the stent and rigid cylinders at each step of the modeling scheme.

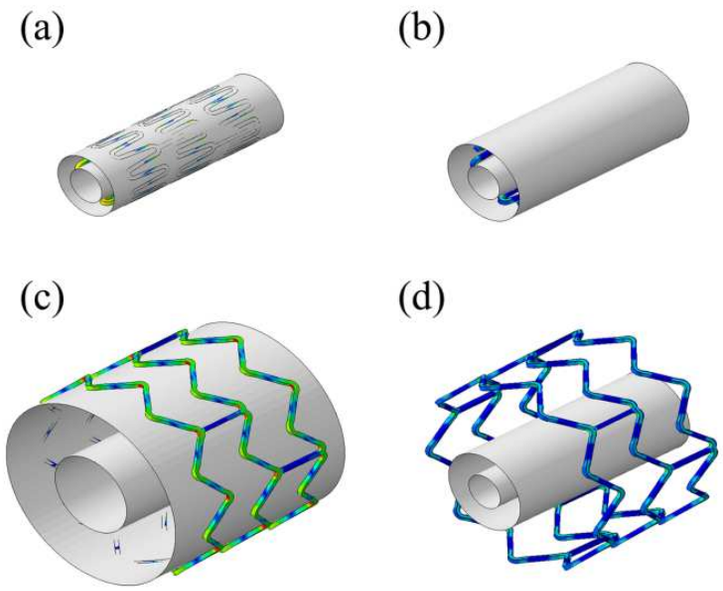

Figure 4. Configuration of the stent/cylindrical surfaces at each stage of the loading scheme: (a) crimp, (b) crimp-recoil, (c) expansion, and (d) expansion-recoil.

3.2.5. Stent Goodman life analysis

Following the previous four steps, systolic/diastolic arterial blood pressures of 180/80 mmHg were applied to simulate the pulsatile fatigue loading. In order to account for the external loading exerted by the arterial wall, an arterial pressure loading corresponding to the interaction between the stent and the artery was also imposed on the stent. The Goodman life analysis was performed using the multi-axial stress state experienced during the pulsatile fatigue loading to determine the fatigue resistance of a stent after implant [14]. It states that fatigue failure will occur if the stress state satisfies the following relationship:

$$\left(\frac{\sigma_a}{\sigma_e}\right)+\left(\frac{\sigma_m}{\sigma_u}\right)\geq 1 \tag{1}$$

where σ_a is the stress amplitude applied to the stent, σ_e is the modified material endurance limit for nonzero mean stress, σ_m is the mean stress applied to the stent, and σ_u is the material ultimate strength.

The Goodman diagram is a plot of the normalized stress amplitude σ_a/σ_e (on the y-axis) versus the normalized mean stress σ_m/σ_u (on the x-axis). The equation $(\sigma_a/\sigma_{e)+}(\sigma_m/\sigma_u)=1$ represents the failure line on the Goodman diagram for nonzero mean stress with the modified endurance limit defined as:

$$\sigma_e = \sigma_{e0}\left(1-\frac{\sigma_m}{\sigma_u}\right) \tag{2}$$

where σ_{e0} is the material endurance limit for zero mean stress. The fatigue safety factor (FSF) is defined as the ratio of the modified endurance limit divided by the stress amplitude. An FSF smaller than 1.0 indicates the fatigue failure:

$$FSF = \frac{\sigma_e}{\sigma_a} \tag{3}$$

4. Depot stent manufacturing

4.1. Laser cutting by integrated laser module

When making a stent, a design drawing is first sketched on the 2D plane, wrapped around a target cylinder, and coded into the 3D cylindrical coordinate using the CAD/CAM software. The coded stent geometry is then input into the laser cutting machine and the design pattern is cut onto a seamless hypotube of 1–2 mm. During the laser cutting process, the hypotube was rotated and translated in the axial direction by the motor stage while the laser source remained stationary.

In this study, a laser module consisting of a 100W Yb-doped pulsed fiber laser (Rofin-Baasel Taiwan Ltd.), a linear X-Y motor stage (Aerotech, Inc.), and a Z-direction server motor was assembled and integrated (Figure 5). The precision motor stage provides linear motion and rotation of the hypotube, whereas the Z-direction server motor controls the distance between the laser source and hypotube surface for the optimal focal position (Figure 6). The X-Y motor stage accuracy is ±2 μm and ±25 arc-second in the axial and circumstantial direction, respectively; on the other hand, the linear encoder resolution for the Z-direction server motor is up to 0.5 μm. Position synchronized output (PSO), a control algorithm that greatly enhances the efficiency and quality of the laser cutting, was used to coordinate the linear X-Y motor stage with the timing of laser firing. It can minimize the heat-affected zone (HAZ) during the laser cutting process. A3200 controller (Aerotech, Inc.) allows us to perform up to 32 axes of synchronized motion control and therefore could accomplish very sophisticated laser cutting patterns effortlessly.

The principles of laser cutting and drilling are based on fusion cutting, which involves a melting mechanism where the heated materials transformed into a molten state are expelled

http://dx.doi.org/10.5772/61790

from the cut kerf by a high pressure assisted gas such as nitrogen or argon. Laser cutting quality is typically controlled by several input laser parameters such as focal position, average laser power, pulse repetition rate, assisted gas pressure, etc. An appropriate position of the laser focal spot significantly improves the cutting outcome. The focal position of our laser module was assessed by measuring the kerf width on the hypotube while adjusting the distance between the laser source and hypotube surface. The smallest kerf width can be achieved by precisely focusing the laser sweet spot on the hypotube surface. A proper selection of laser power is crucial to the outcome as well, as excessive laser power results in a wider kerf and a thicker recast layer. On the other hand, insufficient laser power produces dross due to incomplete melting [21, 22]. Pulse repetition rate is another important laser parameter related to surface roughness and material removal. A higher pulse repetition rate corresponds to a better cutting surface and more effective material removal. Inert gas is a favorable assisted gas since it can avoid oxidation of the materials. High pressure inert gas was used during the cutting process to enhance drag forces and achieve high cutting quality [23].

Figure 5. Integrated laser module with a magnified view of the linear X-Y motor stage and laser source in the right window.

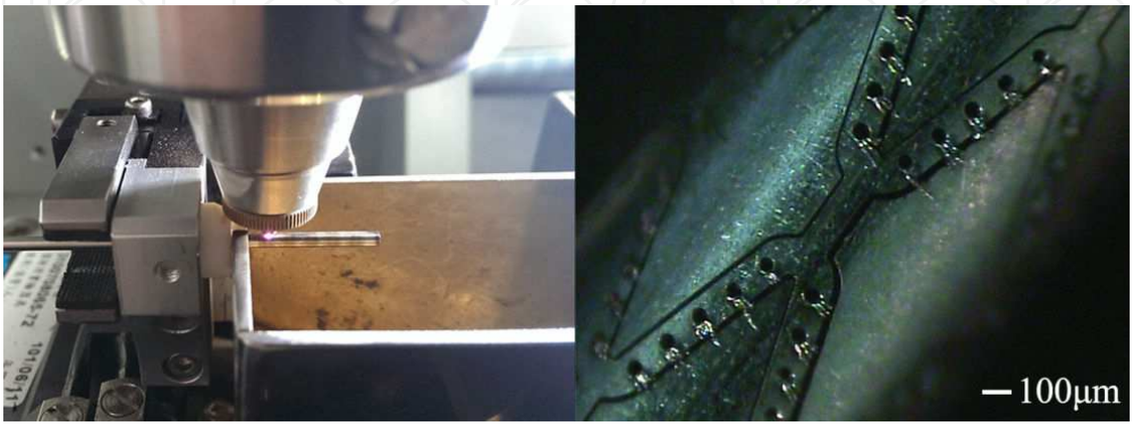

Figure 6. Stent design pattern cut onto a seamless hypotube by laser.

4.2. Surface finishing by electro-polishing

The laser cutting process inevitably generates dross, heat-affected zone, and other defects at stent surface. To achieve high quality of mirror-like surface, electro-polishing was performed on laser-cut depot stent prototypes. A 100 ml glass beaker was used as a bath. The experiment setup used for electro-polishing is illustrated in Figure 7. The stent was used as an anode, whereas the cathode was made of a thin lead sheet. The electrolyte consisted of 60 wt% phosphoric acid (H_3PO_4), 20 wt% sulfuric acid (H_2SO_4), and 20 wt% distilled water. Electro-polishing process was performed with continuous stirring of electrolyte to prevent oxygen bubbles from adhering to stent surface. Furthermore, several important polishing parameters including bath temperature, current, and time were determined through experiments to find the optimal conditions for electro-polishing of depot stents. The stents were then cleaned ultrasonically using distilled water for 5 minutes and were dried by air blowing as the final step.

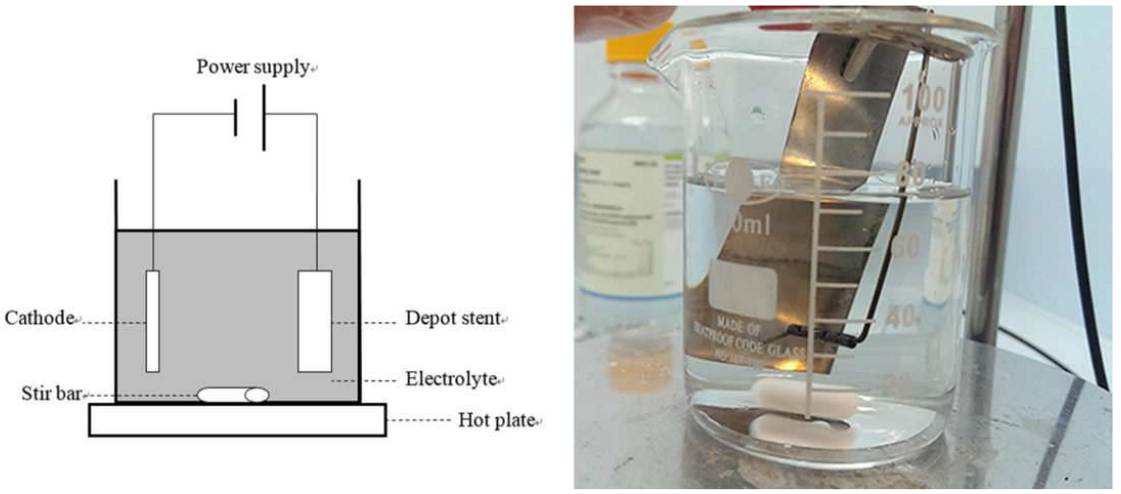

Figure 7. Experimental setup for electro-polishing of depot stent prototypes.

5. Results and discussion

5.1. Effects of reservoir location on stent mechanical integrity

The "standard" stent was first evaluated to establish the baseline information for this study. The FEA simulation was then conducted to investigate the impact of reservoir location on the mechanical integrity of the depot stent (e.g., equivalent plastic strain, radial strength, and fatigue safety factor). Five equally spaced circular (cylindrical if considering depth) and blind-hole reservoirs were cut on three major locations of the depot stent, namely, connectors, bar arms, and crowns (Figure 3).

From Table 1, it is clear that the creation of blind-hole reservoirs on either bar arms or connectors resulted in little or no change in equivalent plastic strain and radial strength. However,

http://dx.doi.org/10.5772/61790

the degradation in the fatigue safety factor was the most significant among major clinical attributes investigated, with a 16–18% reduction compared to the "standard" stent. This indicates that the depot stent with reservoirs on the bar arms or connectors is resistant to vessel collapse or acute stent fracture but susceptible to long-term stent fatigue failure. In other words, the depot stent is more sensitive to dynamic loading than static loading.

However, the depot stent with blind-hole reservoirs on the crowns led to noticeable changes in equivalent plastic strain (+12%) and radial strength (–8%). Its fatigue safety factor declined further from the standard case of 3.05 to 2.33, a significant 24% reduction. By comparing these three reservoir locations, it is clear that cutting reservoirs on the stent crowns has the most significant impact among the three major locations investigated. This is not surprising considering the standard case that the maximum von Mises stress and maximum equivalent plastic strain always occur on the inner surface of the curved crowns, whereas the connectors and the bar arms are mostly under elastic deformation.

Model	RS (N/mm)	Variation (%)	PEEQ (%Strain)	Variation (%)	FSF	Variation (%)
Standard	3.78	-	40.5	-	3.05	-
Hole- CO	3.77	-0.26	40.2	-0.74	2.56	-16.07
Hole- BA	3.66	-3.17	39.7	-1.98	2.49	-18.36
Hole- CR	3.49	-7.67	45.2	11.6	2.33	-23.61
Hole- All	3.45	-8.73	45.1	11.36	2.17	-28.85

Table 1. Effects of reservoir location on stent mechanical integrity (blind-hole reservoirs).

Adding the number of reservoirs increases the total drug capacity of the depot stent. Therefore, investigation was also conducted for reservoirs evenly spread on the entire stent to understand whether the mechanical integrity of such a stent is further compromised or not (Figure 3(d)). Simulation results show that this specific depot stent followed a similar trend to the previous case (blind-hole reservoirs on the crowns only). Their equivalent plastic strain and radial strength were almost identical, whereas the fatigue safety factor continued to decline further, with a 29% reduction compared to the "standard" stent. This again demonstrates that the mechanical integrity of the depot stent is mainly dominated by the reservoirs located on the stent crowns.

5.2. Effects of reservoirs depth on stent mechanical integrity

Another method of increasing the total drug capacity is to cut through-holes instead of blind-holes into the stent struts. The through-hole reservoir design also allows different types of drugs with different release rates to be administered independently on opposite sides of the stent. Since this dual-side drug delivery concept is quite interesting, simulation was then carried out to investigate the effects of reservoir depth on the mechanical integrity of the depot

stent. The depth of the reservoirs was increased from 50% to 75% and 100% of the strut thickness, with the last case equivalent to the through-hole scenario.

Table 2 summarizes the effects of reservoir depth on the key stent attributes for the case of depot reservoirs evenly spread on the entire stent. Figures 8 and 9 show the contour plot comparisons of the equivalent plastic strain developed during different stages of the loading process (crimping and expansion, respectively) between the standard case and the depot stent with through-hole reservoirs on the entire stent. It shows again that the maximum equivalent plastic strain occurred on the inner surface of the most critical region of the stent, the curved crowns. The maximum equivalent plastic strain was increased by 16%, and its strain distribution, as indicated by the colors, changed significantly due to the appearance of the through-hole reservoirs on the stent crowns. It was more evenly spread along the crown arc for the standard case but became non-uniform when the maximum stress–strain occurred at the 6 o'clock location of each reservoir.

Model	RS (N/mm)	Variation (%)	PEEQ (%Strain)	Variation (%)	FSF	Variation (%)
Standard	3.78	-	40.5	-	3.05	-
Hole- All (50%)	3.45	-8.73	45.1	11.36	2.17	-28.85
Hole- All (75%)	3.33	-11.9	46.8	15.56	2.06	-32.46
Hole- All (100%)	3.08	-18.52	46.8	15.56	2.02	-33.77

Table 2. Effects of reservoir location on stent mechanical integrity (blind-hole reservoirs).

Figure 10 shows the radial strength comparison between the "standard" stent and the depot stent with through-hole reservoirs on the entire stent. The radial strength dropped by 19% in this case, and its peak value shifted toward the right by 0.1 mm when compared to the "standard" stent. This suggests that the through-hole depot stent is not as strong as its standard counterpart and could be collapsed by the arterial pressure at an earlier stage. Figure 11 shows the Goodman diagram comparison of the pulsatile fatigue loading between the "standard" stent and the depot stent with through-hole reservoirs on the entire stent. Simulation data of the "standard" stent were far below the Goodman diagram failure line, indicating that the "standard" stent is able to pass the fatigue life of 4×10^8 cycles with ease under pulsatile fatigue loading. Comparing Figure 11 (top) with Figure 11 (bottom), wherein the same stent but with through-hole reservoirs was evaluated for pulsatile fatigue loading, shows that the simulation data of the depot stent migrated toward the Goodman diagram failure line, indicating a significant drop of 34% in FSF and thus much lower fatigue resistance to systolic/diastolic blood pressures in this specific case.

http://dx.doi.org/10.5772/61790

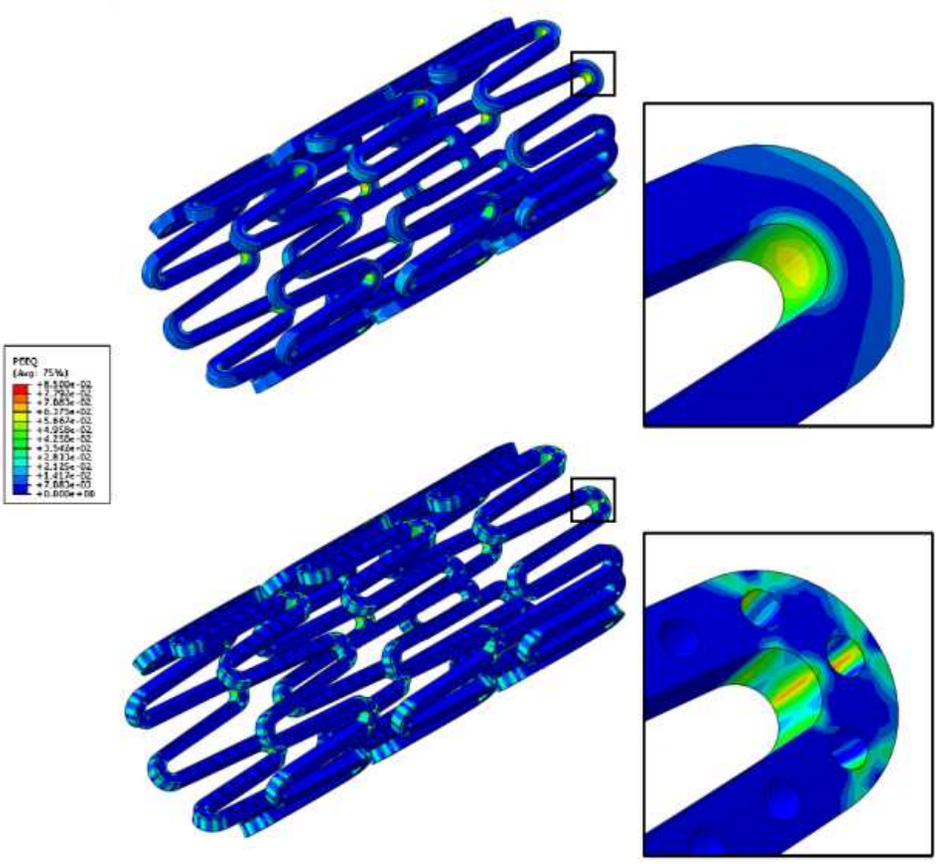

Figure 8. Contour plot of the PEEQ of the standard stent (top) and the depot stent with through-hole reservoirs (bottom) at crimping with a magnified view of the stent crown in the right window.

Figure 12 shows the effects of reservoir depth on the key stent attributes of the depot stent with the reservoir depth ranging from 50%, 75% to 100% of the strut thickness on the entire stent. It is shown that the radial strength decayed almost linearly with the reservoir depth. The loss in radial strength reached the maximum, a 19% reduction compared to the standard case, when the reservoirs were completely cut through. The equivalent plastic strain rose moderately with the reservoir depth but eventually reached a plateau for an approximately 15–20% gain. The fatigue safety factor remained the most critical factor among these key stent attributes. According to the chart, it fell significantly right from the beginning, even with shallow blind holes, but eventually reached a plateau and settled with an approximately 30–35% loss when compared to the standard case. Since the major stent clinical attributes suffered significant losses, it is not a good idea to pursue this specific design with through-hole reservoirs spread all over the entire stent. Given the fact that the crown is a critical region in a stent, we propose that an optimal depot stent should have through-hole reservoirs on the stent bar arms and/or connectors for the maximum drug capacity without compromising its mechanical integrity significantly. It should be noted that although the depot stent has the wonderful feature of precise and programmable drug release control, it was found that its fatigue safety factor could be compromised to certain degrees for all various forms of the depot stent.

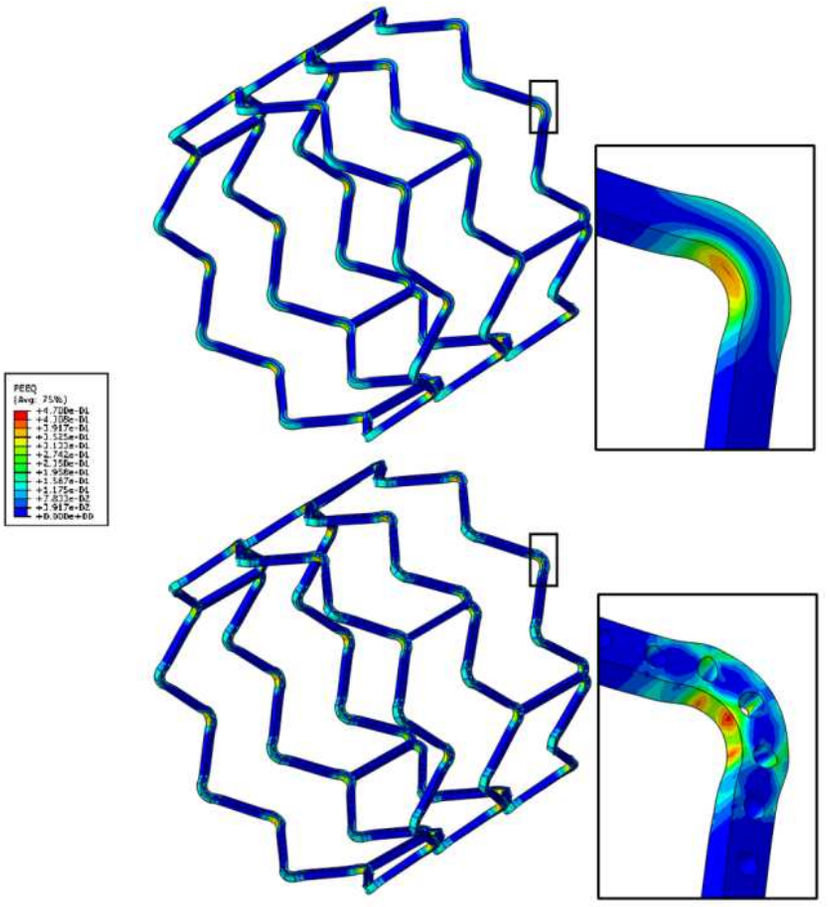

Figure 9. Contour plot of the PEEQ of the standard stent (top) and the depot stent with through-hole reservoirs (bottom) at expansion with a magnified view of the stent crown in the right window.

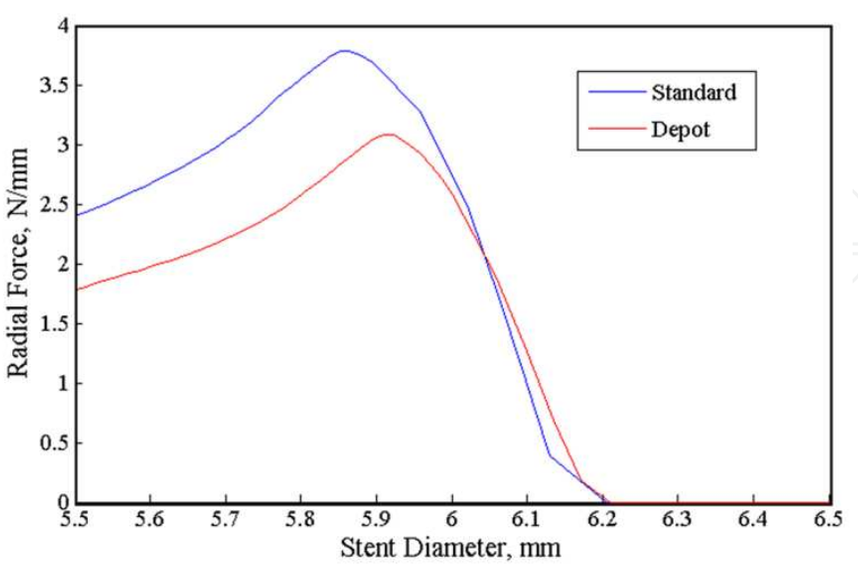

Figure 10. Radial strength comparison of the standard stent and the depot stent with through-hole reservoirs.

http://dx.doi.org/10.5772/61790

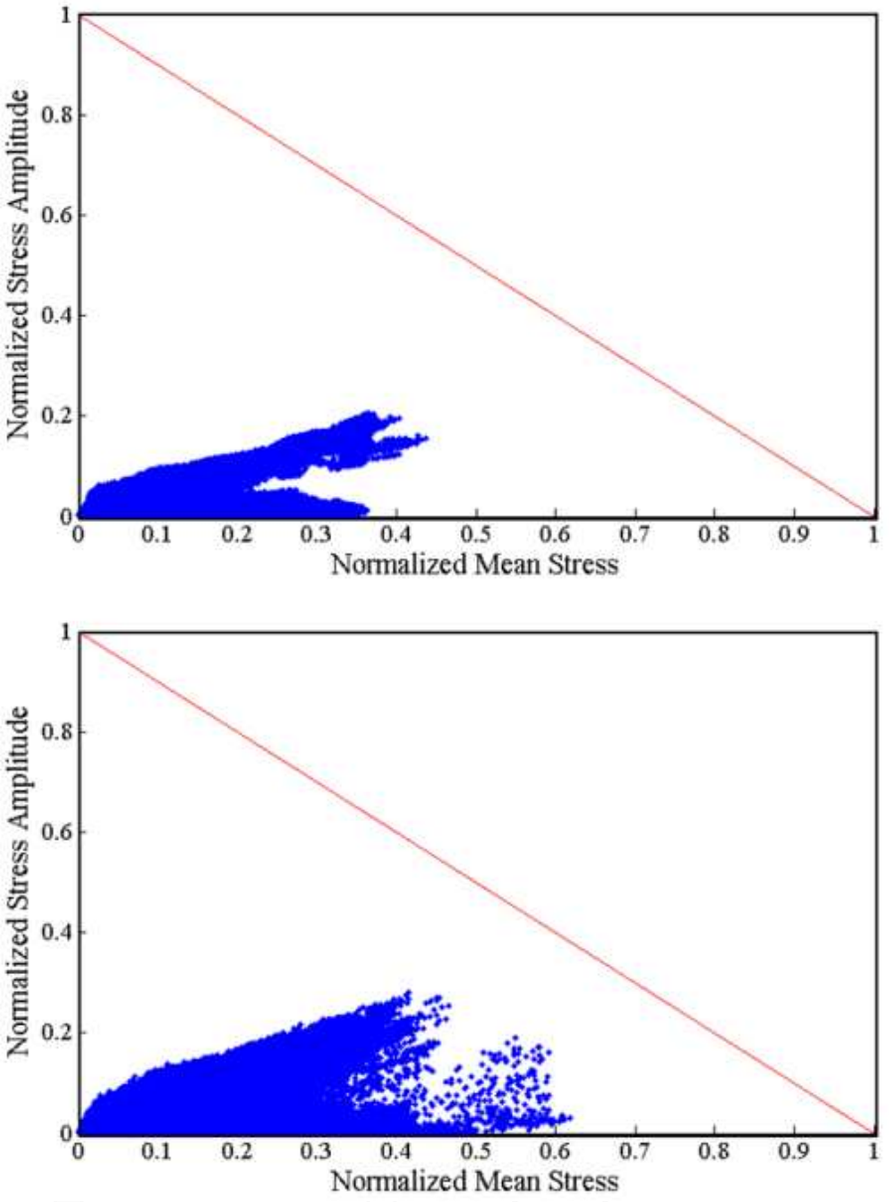

Figure 11. Goodman diagram comparison of the standard stent (top) and the depot stent with through-hole reservoirs (bottom).

5.3. Depot stent drug capacity

A typical DES (3-ring model) with a 5 μm coating thickness carries a total drug-polymer volume of 0.0535 mm^3 (Table 3). For the depot stent, our chosen reservoir size is 50% of the strut width and 100% completely through the strut thickness. Such a design is able to carry approximately 0.0004 mm^3 of drug-polymer mix per reservoir. Therefore, by creating 135 through-hole reservoirs on the 3-ring depot stent model, its total reservoir capacity is enough to fully replace the surface coating layers of 0.0535 mm^3 on a typical drug-eluting stent. This helps to completely eliminate the surface coating layers and thus reduce the overall stent profile.

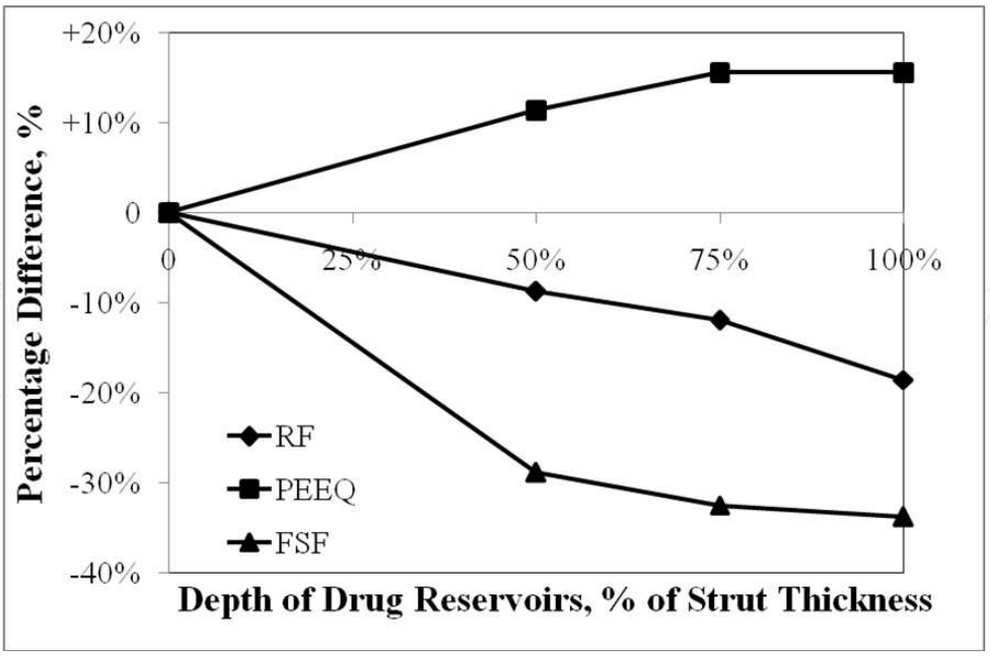

Figure 12. Variation of key clinically relevant functional attributes versus drug reservoir depth.

The density and size of the reservoirs could be changed to increase the total drug capacity of the depot stent. For example, the total volume of the drug-polymer mix can be quadrupled to 0.221 mm^3 when the through-hole reservoirs are evenly distributed on the entire stent, as shown in Figure 3(d). Our proposed depot stent in the next section, same stent as the one in Figure 3(d) without reservoirs on the crowns, also triples the total volume to 0.149 mm^3.

Model	Number of reservoirs	Drug-polymer compound carried (mm^3)
5-μm thickness coating on stent surface	-	0.0535
Through-hole reservoir (per reservoir)	-	0.0004
Through-hole reservoirs on CO	30	0.012
Through-hole reservoirs on BA	270	0.108
Through-hole reservoirs on CR	270	0.108
Through-hole reservoirs on entire stent	552	0.221
Proposed depot stent	372	0.149

Table 3. Estimated drug capacity of a depot stent (3-ring model).

5.4. Proposed depot stent and its variations

5.4.1. Proposed depot stent

We propose an optimal depot stent, with reservoirs uniformly distributed on the entire stent except the crown region, to increase the total drug capacity without comprising its mechanical

integrity significantly (Figure 13). This depot stent has eight reservoirs on the connectors and six reservoirs on the bar arms, with the spacing of approximately 0.15 mm between two reservoirs. Simulation results on the variations of major clinical attributes are listed in Tables 4 along with those on other stents for comparison. Figure 14 shows the contour plot comparison of the equivalent plastic strain developed at the expansion stage among the standard case, the depot stent with through-hole reservoirs on the entire stent, and the proposed depot stent. For the proposed depot stent, the maximum equivalent plastic strain was actually reduced by 9% and the strain distribution was spread out even more uniformly than the standard case. This was attributed to the creation of through-hole reservoirs on the bar arms, effectively shifting the stress–strains away from the crown reservoirs and re-distributing them along the crown arcs. The radial strength only dropped by 10%. The fatigue safety factor was reduced marginally by 13% when compared to the standard case, whereas the very same stent but with through-hole reservoirs on the entire stent showed a staggering 34% reduction. This significant gain in fatigue safety factor was partially due to the removal of through-hole reservoirs on the crowns and partially due to the stress–strain redistribution mentioned above.

To sum up, the total drug capacity of our proposed depot stent could be tripled, with only marginal trade-off in major clinical attributes: its radial strength and the fatigue safety factor were reduced by only 10% and 13%, respectively. Therefore, this depot stent could carry more drugs and deliver them more smartly than the modern drug-eluting stents, thereby opening up a wide variety of new treatment opportunities such as the renal disease or cancer target therapy.

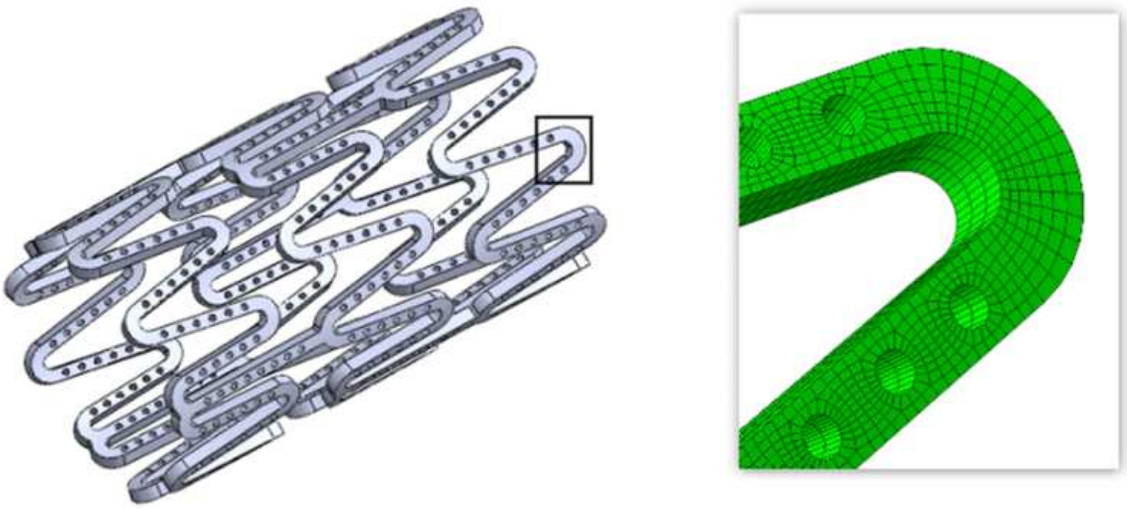

Figure 13. Proposed depot stent with a magnified view of the stent mesh in the right window.

5.4.2. Effects of reservoir shape

Besides the circular (cylindrical if considering depth) reservoirs aforementioned, other reservoir shapes were also investigated, for example, hexagonal and square reservoirs (Figure

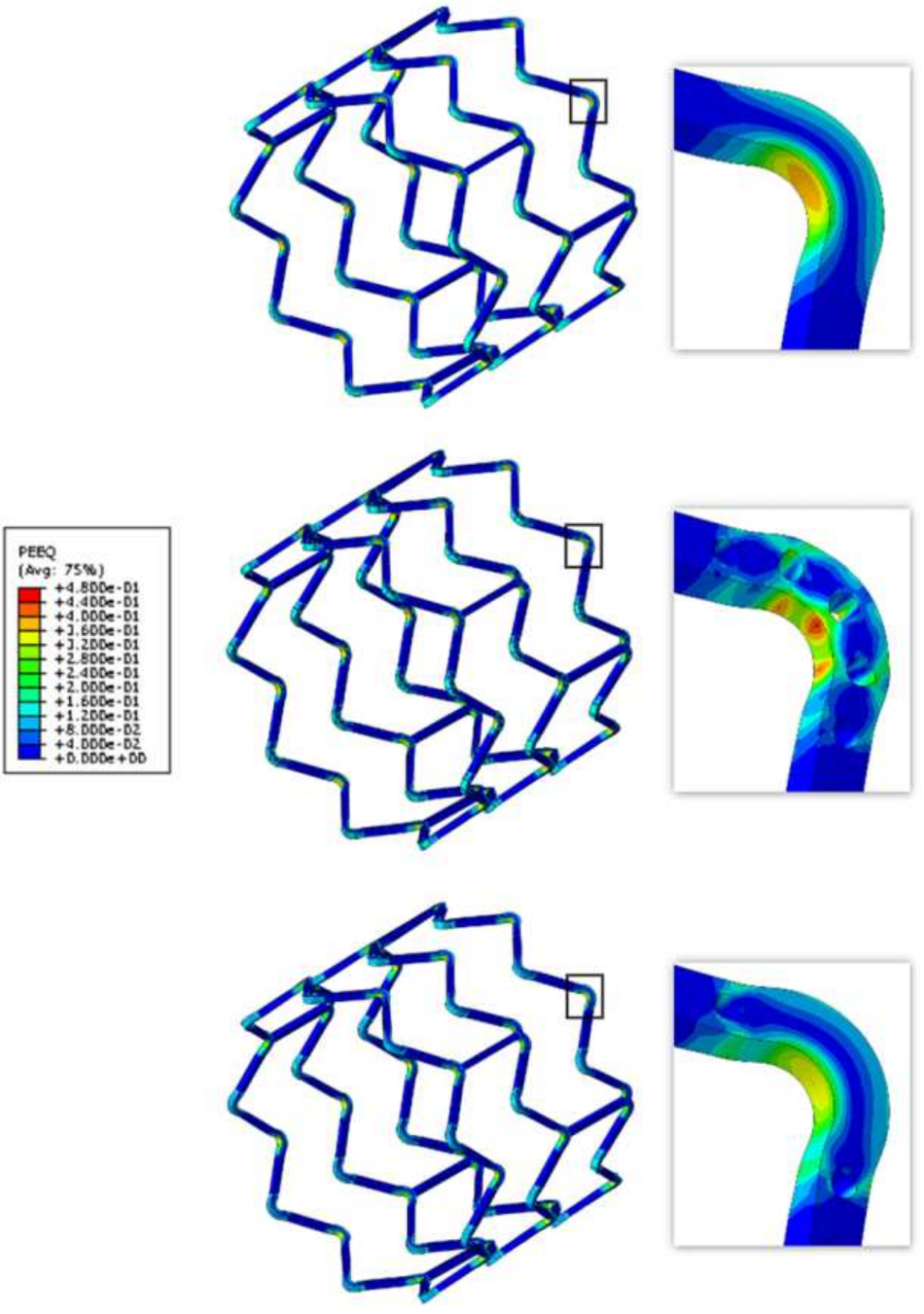

Figure 14. Contour plot of the equivalent plastic strain of the standard stent (top), the depot stent with reservoirs on the entire stent (middle), and the proposed depot stent (bottom) at expansion with a magnified view of the stent crown in the right window.

15). The length on each side of the hexagonal and square reservoirs (0.0349 mm and 0.0563 mm, respectively) was determined in a way that each reservoir capacity was identical to that of a circular reservoir. The location of the reservoir center remained unchanged.

Table 4 lists the mechanical integrity of the depot stent as a function of the reservoir shape. Simulation results show that the changes in the reservoir shape caused little differences in

equivalent plastic strain and radial strength, with approximately 10% across-the-board reductions when compared to the "standard" stent. In terms of the fatigue safety factor, the hexagonal reservoir had a slight 5% advantage over the circular and square reservoirs. This could be attributed to the stress re-distribution within the stent and the hexagonal reservoir makes a bigger impact than reservoirs with other shapes.

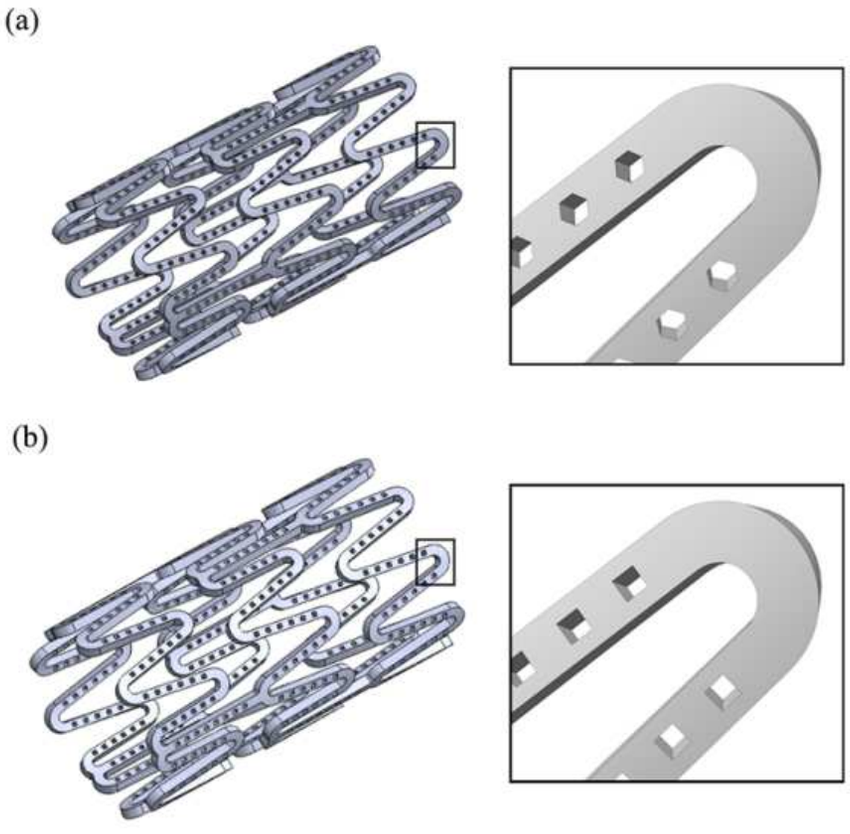

Figure 15. Depot stent with (a) hexagonal and (b) square reservoirs.

Model	RS (N/mm)	Variation (%)	PEEQ (%Strain)	Variation (%)	FSF	Variation (%)
Standard	3.78	-	40.5	-	3.05	-
Proposed depot stent	3.41	-9.79	36.7	-9.38	2.66	-12.79
Hexagonal reservoir	3.43	-9.26	36.4	-10.12	2.80	-8.20
Square reservoir	3.38	-10.58	36.1	-10.86	2.65	-13.11

Table 4. Effects of reservoir shape on stent mechanical integrity.

5.4.3. Effects of reservoir size and number

Effects of the reservoir size and number of the depot stent were also investigated (Figure 16). The total drug loading capacity on each bar arm/connector was intended to maintain the same,

whereas the size and number of the reservoirs were adjusted accordingly. Stent variation #1 had smaller but more reservoirs, with 8 reservoirs on the bar arms and 10 reservoirs on the connectors; on the other hand, stent variation #2 had larger but fewer reservoirs, with four reservoirs on the bar arms and six reservoirs on the connectors. In all cases, the total length between the farther edges of two end reservoirs remained unchanged.

Table 5 lists the mechanical integrity of the depot stent as a function of the reservoir size and number. Simulation results show that, for the same drug loading capacity, stent variation #2 with larger and fewer reservoirs yielded lower radial strength, but smaller equivalent plastic strain and thus higher fatigue safety factor. In addition, the fatigue safety factor seems to be more sensitive than the equivalent plastic strain and radial strength in this case. Its value increased from 2.36 to 2.88, a 17% jump from stent variation #1 to #2, which is consistent with the earlier observation. Therefore, stent variation #2 of larger and fewer reservoirs is a better candidate for drug delivery; its total drug capacity could be tripled with marginal trade-off in its major clinical attributes: the radial strength and fatigue safety factor were reduced by only 11% and 6%, respectively.

Model	RS (N/mm)	Variation (%)	PEEQ (%Strain)	Variation (%)	FSF	Variation (%)
Standard	3.78	-	40.5	-	3.05	-
Proposed depot stent	3.41	-9.79	36.7	-9.38	2.66	-12.79
Variation #1	3.48	-7.94	37.6	-7.16	2.36	-22.62
Variation #2	3.38	-10.58	34.8	-14.70	2.88	-5.57

Table 5. Effects of reservoir size and number on stent mechanical integrity.

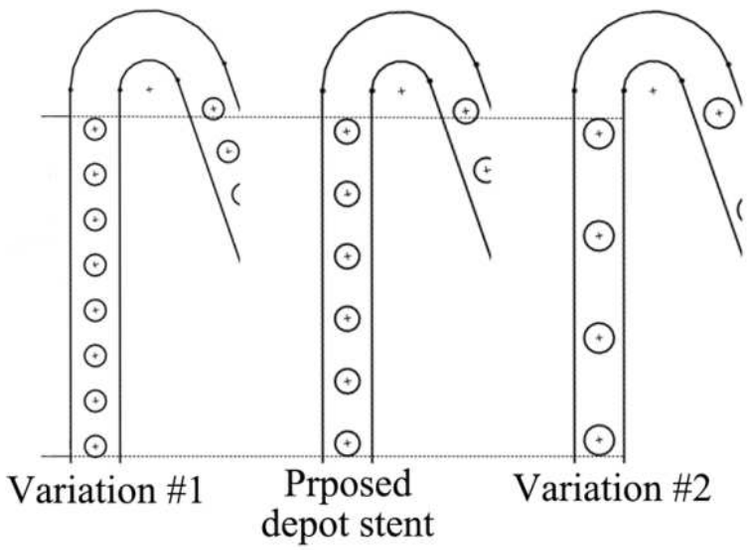

Figure 16. Proposed depot stent and its variation #1 and #2.

http://dx.doi.org/10.5772/61790

5.5. Depot stent prototyping

In this study, the input laser parameters used for cutting stents are listed as follows: average power 37.5 W, pulse repetition rate 80 KHz, cutting speed 5 mm/s, and Argon pressure 12 bar. Optical microscopy was used to measure the kerf width and observe the surface conditions of each stent.

Figure 17 shows the relationship of the average kerf width vs. the distance between the laser source and hypotube surface. The kerf width had the minimum value of 23.2 μm at the distance of 0.37 mm. When the distance was between 0.27 mm and 0.51 mm, the laser beam was able to penetrate through the hypotube, resulting in successful cutting within a focal-depth range of 0.24 mm. Figure 6 is the depot stent design pattern cut onto a seamless hypotube by laser prior to material removal and electro-polishing.

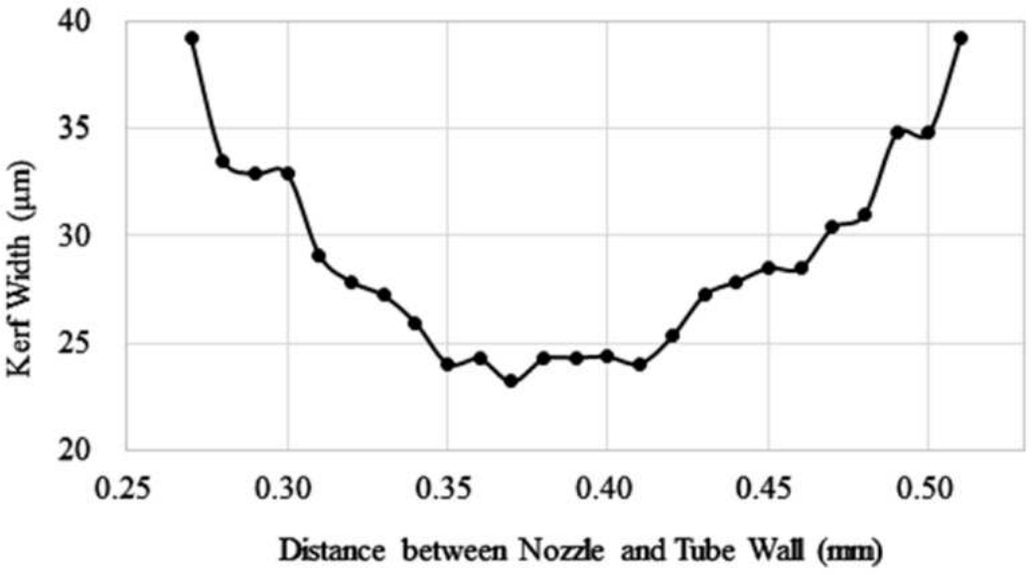

Figure 17. Average kerf width vs. distance between laser source and hypotube surface.

The polishing conditions for surface finishing of depot stent prototypes are listed in Table 6. Figure 18 shows the depot stent prototype before and after electro-polishing. These stents were able to achieve high quality of mirror-like surface finishing after polishing. Figure 19 is the prototype of our proposed depot stent of 2 mm diameter and 22 mm long for demonstration of our design concept.

Stirring speed (RPM)	Current (A)	Time (sec)	Temperature (°C)
500–550	0.242	105–135	50–55

Table 6. Electro-polishing conditions for surface finishing of depot stents.

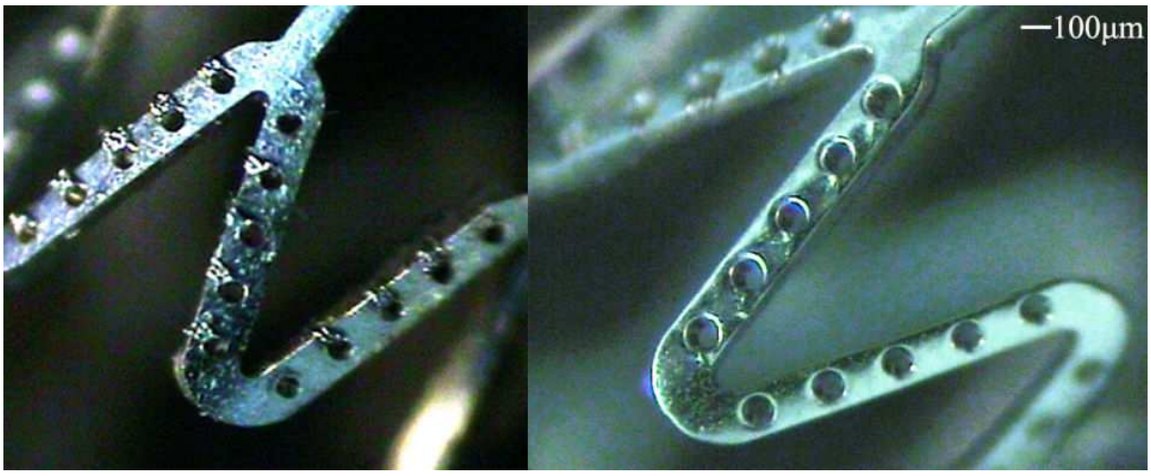

Figure 18. Surface conditions of manufactured depot stents before (left) and after (right) electro-polishing.

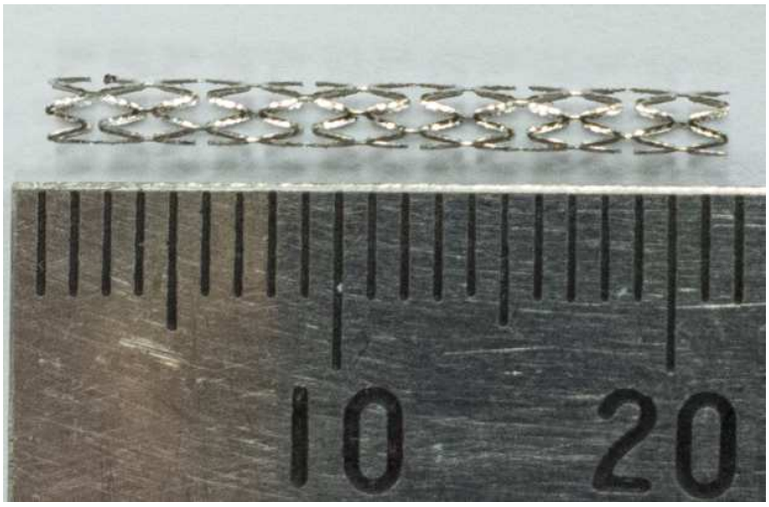

Figure 19. Prototype of our proposed depot stent.

6. Conclusion

The depot stent with micro-sized drug reservoirs is a novel concept for smart drug delivery and provides a promising future for highly controlled release of different medications with programmable spatial/temporal control. However, creating such drug reservoirs on the stent struts inevitably weaken the stent scaffolding and compromise its mechanical integrity. The impact of these drug reservoirs on major clinical attributes of the depot stent was systematically investigated. Several conclusions were drawn from this study:

i. The reservoirs on either bar arms or connectors had little effects in equivalent plastic strain and radial strength when compared to the "standard" drug-eluting stent. However, the fatigue safety factor was reduced more significantly, suggesting that

the depot stent is resistant to acute stent fracture or vessel collapse but susceptible to long-term stent fatigue failure.

ii. Creating reservoirs on the crown region of the depot stent has the most significant impact among all major locations.

iii. The degradation in mechanical integrity is more sensitive to reservoir location than reservoir depth.

iv. The hexagonal reservoirs resulted in a marginal increase in fatigue resistance when compared to the circular and square reservoirs.

v. For the same drug loading capacity, larger and fewer reservoirs resulted in a noticeable increase in the fatigue resistance over smaller and more reservoirs.

vi. Our proposed depot stent was proven to be a feasible design. Its total drug capacity could be tripled with acceptable/marginal trade-off in major clinical attributes: the radial strength and the fatigue safety factor of our proposed depot stent were reduced by only 10% and 13%, respectively.

vii. A prototype of our proposed depot stent (2 mm diameter and 22 mm long) was manufactured for the feasibility demonstration of our design concept.

This study can serve as a guideline to help future depot stent designs to achieve the best combination of stent mechanical integrity and smart drug delivery.

Acknowledgements

This research was supported by the Ministry of Science and Technology in Taiwan through Grants MOST-103-2622-E-002-010-CC1 and NSC-102-2221-E-002-130-MY3. The authors are grateful for the support and help.

Author details

Hao-Ming Hsiao[1*], Aichi Chien[2], Bor-Hann Huang[1], Dian-Ru Li[3], Hsin Chen[4] and Chun-Yi Ko[1]

*Address all correspondence to: hmhsiao@ntu.edu.tw

1 Department of Mechanical Engineering, National Taiwan University, Taipei, Taiwan

2 Department of Radiology, University of California, Los Angeles, CA, USA

3 Department of Mechanical Engineering, University of Michigan, Ann Arbor, MI, USA

4 Department of Mechanical Engineering, Stanford University, Stanford, CA, USA

References

[1] M. R. Bell, P. B. Berger, J. F. Bresnahan, G. S. Reeder, K. R. Bailey, and D. Holmes, "Initial and long-term outcome of 354 patients after coronary balloon angioplasty of total coronary artery occlusions," *Circulation,* vol. 85, pp. 1003-1011, 1992.

[2] C. Landau, R. A. Lange, and L. D. Hillis, "Percutaneous transluminal coronary angioplasty," *New England Journal of Medicine,* vol. 330, pp. 981-993, 1994.

[3] B. L. Van der Hoeven, N. M. Pires, H. M. Warda, P. V. Oemrawsingh, B. J. van Vlijmen, P. H. Quax*, et al.*, "Drug-eluting stents: results, promises and problems," *International Journal of Cardiology,* vol. 99, pp. 9-17, 2005.

[4] M.-C. Morice, P. W. Serruys, J. E. Sousa, J. Fajadet, E. Ban Hayashi, M. Perin*, et al.*, "A randomized comparison of a sirolimus-eluting stent with a standard stent for coronary revascularization," *New England Journal of Medicine,* vol. 346, pp. 1773-1780, 2002.

[5] J. W. Moses, M. B. Leon, J. J. Popma, P. J. Fitzgerald, D. R. Holmes, C. O'Shaughnessy*, et al.*, "Sirolimus-eluting stents versus standard stents in patients with stenosis in a native coronary artery," *New England Journal of Medicine,* vol. 349, pp. 1315-1323, 2003.

[6] A. Colombo and E. Karvouni, "Biodegradable stents "fulfilling the mission and stepping away"," *Circulation,* vol. 102, pp. 371-373, 2000.

[7] H. R. Kricheldorf, I. Kreiser-Saunders, C. Jürgens, and D. Wolter, "Polylactides-synthesis, characterization and medical application," *Macromolecular Symposia*, pp. 85-102, 1996.

[8] J. A. Ormiston and P. W. Serruys, "Bioabsorbable coronary stents," *Circulation: Cardiovascular Interventions,* vol. 2, pp. 255-260, 2009.

[9] T. Tsuji, H. Tamai, K. Igaki, E. Kyo, K. Kosuga, T. Hata*, et al.*, "Biodegradable stents as a platform to drug loading," *International Journal of Cardiovascular Interventions,* vol. 5, pp. 13-16, 2003.

[10] R. Waksman, "Biodegradable stents: they do their job and disappear," *The Journal of Invasive Cardiology,* vol. 18, pp. 70-74, 2006.

[11] R. Blindt, K. Hoffmeister, H. Bienert, G. Bartsch, H. Thissen, D. Klee*, et al.*, "Development of a new biodegradable intravascular polymer stent with simultaneous incorporation of bioactive substances," *The International Journal of Artificial Organs,* vol. 22, pp. 843-853, 1999.

[12] P. W. Serruys, G. Sianos, A. Abizaid, J. Aoki, P. den Heijer, H. Bonnier*, et al.*, "The effect of variable dose and release kinetics on neointimal hyperplasia using a novel

paclitaxel-eluting stent platform: the Paclitaxel In-Stent Controlled Elution Study (PISCES)," *Journal of the American College of Cardiology,* vol. 46, pp. 253-260, 2005.

[13] A. Finkelstein, D. McClean, S. Kar, K. Takizawa, K. Varghese, N. Baek, *et al.*, "Local drug delivery via a coronary stent with programmable release pharmacokinetics," *Circulation,* vol. 107, pp. 777-784, 2003.

[14] H.-M. Hsiao, Y.-H. Chiu, K.-H. Lee, and C.-H. Lin, "Computational modeling of effects of intravascular stent design on key mechanical and hemodynamic behavior," *Computer-Aided Design,* vol. 44, pp. 757-765, 2012.

[15] H.-M. Hsiao, C.-T. Yeh, C. Wang, L.-H. Chao, and D.-R. Li, "Effects of stent design on new clinical issue of longitudinal stent compression in interventional cardiology," *Biomedical Microdevices,* vol. 16, pp. 599-607, 2014.

[16] H.-M. Hsiao, Y.-H. Chiu, T.-Y. Wu, J.-K. Shen, and T.-Y. Lee, "Effects of through-hole drug reservoirs on key clinical attributes for drug-eluting depot stent," *Medical Engineering & Physics,* vol. 35, pp. 884-897, 2013.

[17] H.-M. Hsiao and M.-T. Yin, "An intriguing design concept to enhance the pulsatile fatigue life of self-expanding stents," *Biomedical Microdevices,* vol. 16, pp. 133-141, 2014.

[18] H. M. Hsiao, A. Nikanorov, S. Prabhu, and M. K. Razavi, "Respiration-induced kidney motion on cobalt-chromium stent fatigue resistance," *Journal of Biomedical Materials Research Part B: Applied Biomaterials,* vol. 91, pp. 508-516, 2009.

[19] M. De Beule, P. Mortier, S. G. Carlier, B. Verhegghe, R. Van Impe, and P. Verdonck, "Realistic finite element-based stent design: the impact of balloon folding," *Journal of Biomechanics,* vol. 41, pp. 383-389, 2008.

[20] F. Gervaso, C. Capelli, L. Petrini, S. Lattanzio, L. Di Virgilio, and F. Migliavacca, "On the effects of different strategies in modelling balloon-expandable stenting by means of finite element method," *Journal of Biomechanics,* vol. 41, pp. 1206-1212, 2008.

[21] L. Shanjin and W. Yang, "An investigation of pulsed laser cutting of titanium alloy sheet," *Optics and Lasers in Engineering,* vol. 44, pp. 1067-1077, 2006.

[22] C. Wandera, "Laser cutting of austenitic stainless steel with a high quality laser beam," LAPPEENRANTA UNIVERSITY OF TECHNOLOGY, 2006.

[23] W. Steen, K. G. Watkins, and J. Mazumder, *Laser material processing*: Springer Science & Business Media, 2010.

IntechOpen